FULL PAPER

Virus-Inspired Mimics Based on Dendritic Lipopeptides for Efficient Tumor-Specific Infection and Systemic Drug Delivery

Zhijun Zhang, Xiao Zhang, Xianghui Xu, Yunkun Li, Yachao Li, Dan Zhong, Yiyan He, and Zhongwei Gu**

Herein, multifunctional mimics of viral architectures and infections self-assembled from tailor-made dendritic lipopeptides for programmed targeted drug delivery are reported. These viral mimics not only have virus-like components and nanostructures, but also possess virus-like infections to solid tumor and tumor cells. Encouragingly, the viral mimics provide the following distinguished features for tumor-specific systemic delivery: i) stealthy surface to resist protein interactions and prolong circulation time in blood, ii) well-defined nanostructure for passive targeting to solid tumor site, iii) charge-tunable shielding for tumor extracellular pH targeting, iv) receptor-mediated targeting to enhance tumor-specific uptake, and v) supramolecular lysine-rich architectures mimicking viral subcellular targeting for efficient endosomal escape and nuclear delivery. This bioinspired design make in vivo tumor suppression by drug-loaded viral mimics against BALB/c mice bearing 4T1 tumor greatly exceed the positive control group (more than three times). More importantly, viral mimics hold great potentials to reduce side effects and decrease tumor metastasis after systemic administration.

1. Introduction

Over the past several decades, wonderful natural systems have continuously inspired scientists to develop excellent mimics of biological structures and functions.[1–4] Viruses, as one of highly evolved nanoparticulate organisms in the nature, are initially explored as virus-based vectors for disease therapy owing to their high infectivity;[5,6] while a number of adverse events caused by virus-based vectors (e.g., toxicity, mutagenesis, and immunogenicity) drive researchers to develop artificial viruses with defined components for efficient and safe therapeutic agent delivery.[7,8] With the better understandings of nature and science, the dream of creating advanced artificial viruses with synthetic building blocks is becoming more realistic.[9–12] In recent years, a series of novel nanoassemblies mimicking viral components and architectures have been well constructed.[13–15] Encouragingly, some morphological and structural mimics of viruses (e.g., capsids, envelopes, and rough surface topography) succeed in enhancement of bioactive molecules delivery efficiency.[16–20] Previously, we reported the virus-inspired fabrications of components simulation and architectural mimic to improve gene transfer efficiency.[21,22] Furthermore, mimicking critical processes of virus infections (e.g., endosomal escape, capsid disassembly, and nuclear delivery) show great potentials to increase bioavailability of antitumor drugs and therapeutic genes.[23–27] We also demonstrated a few biodetachable artificial capsids mimicking the viral disruption in the cytosol for programmed drug and gene delivery.[28,29] However, up to now, the structural and functional mimics of viruses just achieve the modest improvements, and viral advantages including logical infectivity and systemic delivery have not been fully imitated by artificial virus-inspired systems.[10–12]

Although there is still a long way to go from sophisticated structural mimics toward advanced functional simulations, developing a new generation of viral mimics (VMs) as versatile nanovehicles is full of challenges, opportunities, and prospects.[9] On the one hand, both high delivery efficiency and systemic delivery are urgently pursued for virus-inspired vectors,[9–11] because most of current virus-mimicking vectors just show considerable efficiency in vitro and lack of more features (e.g., minimal interactions with blood compartments and long blood circulation) to meet systemic delivery and clinical applications.[16–18,24–27] On the other hand, natural virus-based vectors do not have important capability for tumor-specific recognition (e.g., tumor-targeted delivery and tumor-activated delivery); therefore, integrating the ability of tumor recognition into virus-inspired design offers an important opportunity to build highly efficient vehicles surpassing the functionalities of virus-based vectors.[30] Fortunately, more and more state-of-the-art strategies based on molecular and supramolecular science make possible optimizations of virus-inspired vehicles for in-depth studies and systemic delivery; for examples, biomimetic

Z. Zhang, X. Zhang, Dr. X. Xu, Y. Li, Y. Li, D. Zhong, Dr. Y. He, Prof. Z. Gu
National Engineering Research Center for Biomaterials
Sichuan University
Chengdu, Sichuan 610064, P. R. China
E-mail: xianghui.xu@hotmail.com; zwgu@scu.edu.cn

DOI: 10.1002/adfm.201502049

molecular design, bioinspired supramolecular self-assembly, and tumor-targeted technology.

Specifically speaking, it is reported that design and self-assembly of amphiphilic dendrons/dendrimers into supramolecular dendritic systems is the most promising chemical strategy to generate the latest delivery nanocarriers,[31,32] which have some inherent properties similar to biological envelopes or viral capsids.[21,33] Meanwhile, it can be predicted that if virus-inspired components (e.g., peptides, lipopeptides, and glycopeptide) are used to engineer dendritic molecules as bioinspired building blocks, structural mimics of natural virus will achieve more perfection.[20,21,33] More importantly, many burgeoning progresses on chemistry and biomedicine provide the possibility to endow virus-inspired vectors with virus-like infectivity: (i) purposeful design of building blocks (e.g., PEGylation and negative shielding) to prolong blood circulation mimicking viral systemic infection;[34–36] (ii) the unique tumor extracellular environment (e.g., weakly acidic pH and a high proteinase concentration)[37,38] and overexpressed receptors on tumor cell surface could be explored as tumor-specific targets to build tumor-targeted viral mimics;[39] and (iii) additionally, we find supramolecular dendritic systems self-assembled from the low-generation peptide dendrons offer a new avenue to facilitate endosomal escape and nuclear targeting,[28,40] which are analogous to viral subcellular targeted delivery.[25,27,41,42] Motivated by these inspirations, we believe that with a rational chemical design, ideal mimics of viral structures and functions will be developed as efficient therapeutic delivery platform.

To prove our concept, virus-inspired mimics mimicking the viral components and structures were designed using coassembly of tailor-made building blocks for gaining virus-like systemic infectivity, as well as improving programmed targeted delivery of antitumor agents (**Figure 1**). This type of virus-inspired nanovehicles is expected to offer the following benefits: (1) dendritic molecular structures to mimic globular capsid proteins,[32,43] (2) lipopeptide-based components to simulate the compositions of viral envelope and capsid,[44] (3) stealthy negative corona to obtain virus-like systemic delivery (e.g., minimal protein interactions and long circulation in blood), and hydrophobic core to encapsulate bioactive molecules (e.g., antitumor agents), (4) well-defined nanostructures for passive targeting to solid tumor site by EPR effect, (5) tumor microenvironment–activated surface to enhance tumor extracellular targeting, (6) receptor-mediated targeting via coassembly with synergetic units to enhance tumor-specific cellular uptake mimicking viral internalization, and (7) supramolecular lysine-rich architectures to generate virus-like subcellular targeting (endosomal escape and nuclear targeting). In brief, this bioinspired strategy focuses on the development of superb viral mimics from structural bionics to functional implementation to address some contradictions and difficulties in systemic delivery.

2. Results and Discussion

First, the amphiphilic dendritic lipopeptides (DLPs) were synthesized using the divergent–convergent method, and their peripheral groups (—NH_2) were functionalized with acid-cleavable carboxy groups by 2,3-dimethylmaleic anhydride (DA) into 2,3-dimethylmaleic anhydride-modified dendritic lipopeptides (DA-DLPs).[45–47] As shown in **Figure 2**A, the matrix-assisted laser desorption ionization time-of-flight mass spectroscopy (MALDI-TOF MS) result confirmed the DA-DLPs was successfully obtained with molecular weight of 1534.97 agreed with theoretical value of 1534.03. The detailed synthesis **(**Figures S1 and S2, Supporting Information**)** and characterizations **(**Figures S5–S15, Supporting Information**)**

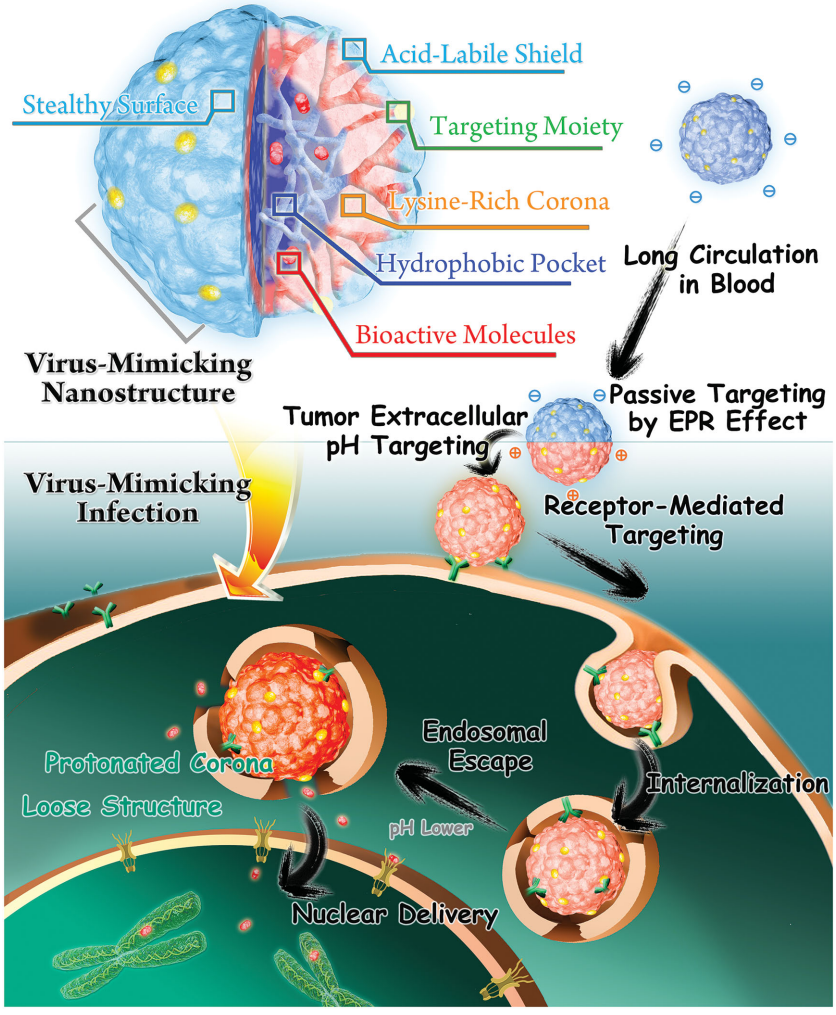

Figure 1. Schematic illustrations for virus-mimicking nanostructures assembled from specially made dendritic lipopeptides, and their virus-mimicking systemic infections for overcoming biological barriers and navigating tumor-specific drug delivery.

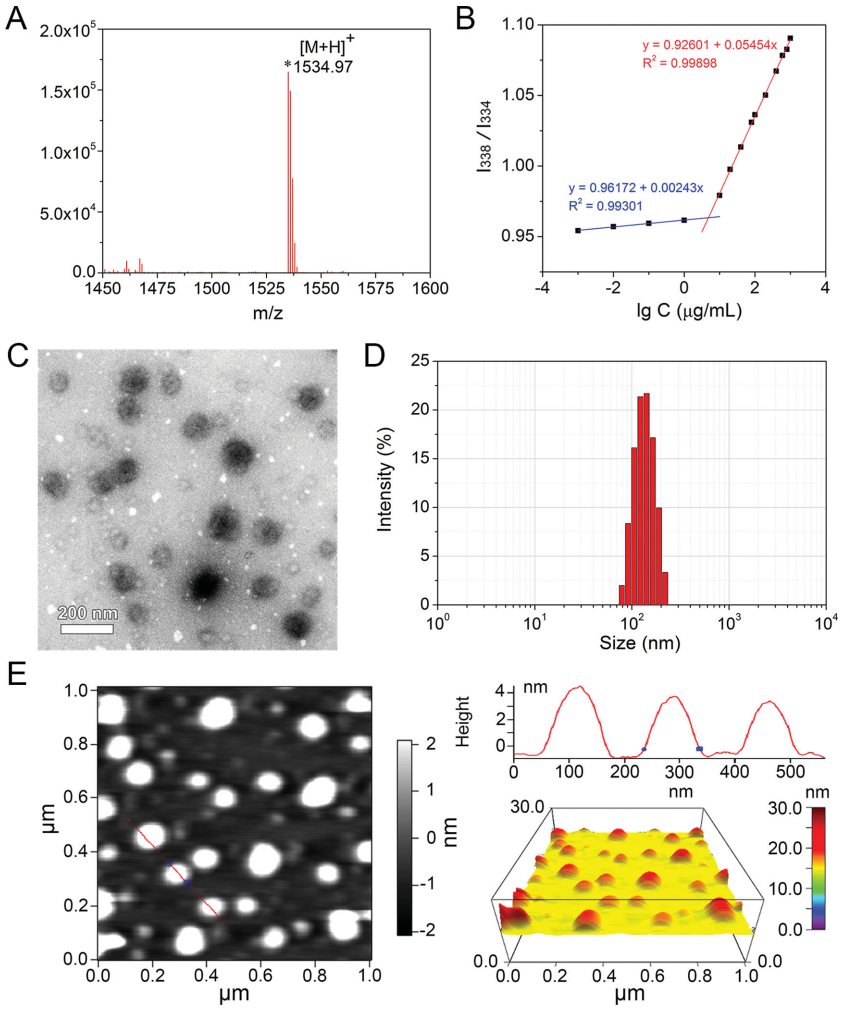

Figure 2. Supramolecular mimics of viral components and structures. A) MALDI-TOF mass spectrum and B) critical assembly concentration of DA-functionalized dendritic lipopeptides. C) TEM image and D) size distribution of viral mimics. E) AFM image for 3D architectures of viral mimics including top view, the size profile along the red line, and 3D view.

of DA-DLPs can be found in the Supporting Information. In aqueous medium, amphiphilic DA-DLPs were able to self-assemble into hierarchical nanostructures with hydrophilic peptide corona and hydrophobic lipid core. The critical assembly concentration (CAC) of DA-DLPs was determined with a low value of 4.85 μg mL^{-1} (Figure 2B). As shown by transmission electron microscopy (TEM, Figure 2C), dendritic lipopeptide–based assemblies presented spherical nanostructures with the diameter ranging from 100 to 200 nm like VMs.[48] An average size of 145.3 ± 2.2 nm was determined by dynamic light scattering (DLS) measurement (Figure 2D). It was noted that these viral mimics had zeta potential of –17.3 mV (Figure S25, Supporting Information). Additionally, atomic force microscopy (AFM) clearly showed 3D architectures of VMs, which were in good agreement with TEM and DLS results (Figure 2E). As viral features for systemic infection, VMs with well-defined nanostructures and negative shelters may be beneficial to resistance to nonspecific protein adsorption, long blood circulation, and passive targeting to solid tumor.

It is known that tumor sites exhibit an average extracellular pH value between 6.0 and 7.0, which is lower than that of normal tissues and blood (around 7.4). Some recent designs on tumor extracellular targeting successfully enhanced the accumulation of nanoparticles at tumor site. Next, we investigated whether slightly acid condition could remove the shelters of charge-conversional VMs (CVMs, self-assembly of DA-DLPs) by some physicochemical characterizations (**Figure 3**A). On the basis of MALDI-TOF mass spectra, the disappearance of the peak at 1534.97 and the appearance of the peak at 1030.86 directly indicated pH 6.8 triggered the hydrolysis of the amide bonds connected with negative shielding (Figure 3B). ^{1}H-NMR spectra also recorded cleavable properties of these amide bonds in DA-DLPs under weakly acidic condition (pH 6.8) in Figure 3C. With pH value adjusted to pH 6.8, the signal of α-H (Ha in Figure 3A, 4.51 ppm) in DA-DLPs decreased, accompanying with the increased signal of Ha′ (3.35 ppm), which should be ascribed to acid-labile cleavages of the amide bonds; and similar conversions happened between Hb (3.21 ppm) in DA-DLPs and Hb′ (2.65 ppm) in DLPs. Furthermore, amino exposure tests demonstrated that CVMs self-assembled from DA-DLPs could stably exist with stealthy shielding at pH 7.4 (Figure 3D). But at pH 6.8, ≈80% of DA-masked primary amines in CVMs were hydrolyzed into the original status with abundant exposed amino groups within 20 min, and the exposure degree of amino groups in CVMs were rapidly close to positively charged viral mimics (PVMs) self-assembled from DLPs. Nevertheless, the negatively charged VMs (NVMs) self-assembled from succinic anhydride–modified DLPs (SA-DLPs), which was much less sensitive to weakly acidic condition as control assemblies, were little hydrolyzed both under pH 7.4 and 6.8. More importantly, the surface charge of CVMs rapidly converted after the hydrolysis of amide bonds (Figure 3E). At pH 7.4 analogous to normal physiological pH condition, CVMs always kept negative charge with zeta potential of around –17.0 mV for 2 h; while at pH 6.8 mimicking tumor extracellular pH, their surface charge fast increased to +8.1 mV within 20 min; furthermore, at pH 5.0 corresponding to pH value of lysosome, the zeta potential of CVMs reached up to +21.3 mV within 20 min. The relatively fast charge conversion should be ascribed to their peripheral charge-tunable groups fully exposed to lower pH environment, distinguishing from charge-conversional side groups in linear polymers.[35,36,45–47] Taken together, CVMs were able to serve as sensitively charge-tunable nanovehicles, because of their negatively charged surface at pH 7.4 to reduce nonspecific protein adsorption, their positively charged surface at pH 6.8 to realize tumor extracellular targeting and enhanced internalization, and

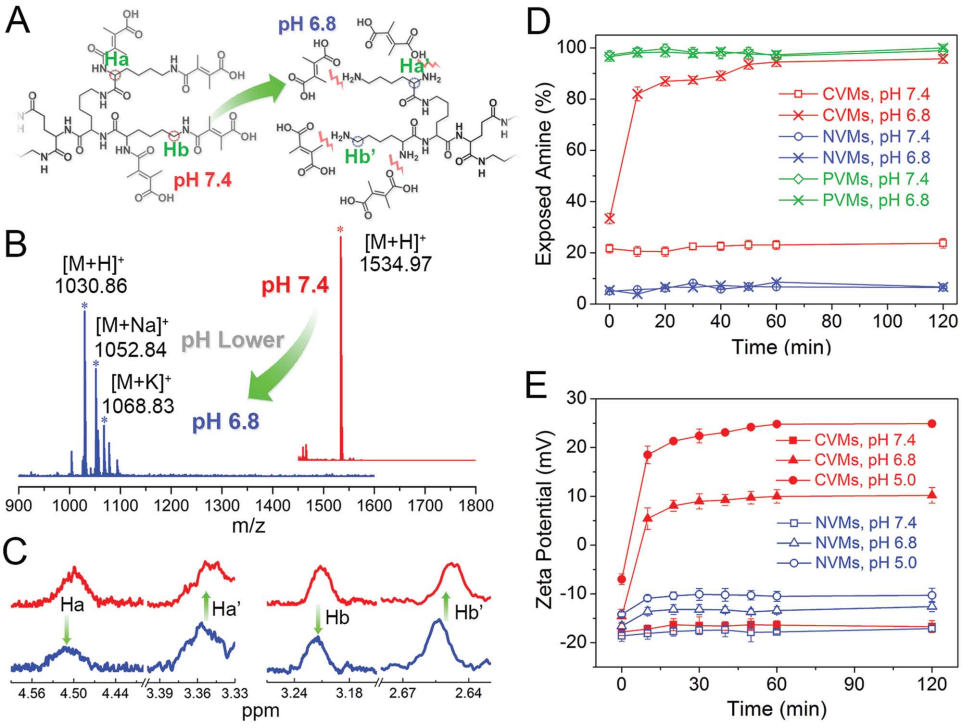

Figure 3. A) Schematic illustration, B) mass spectra, and C) ^{1}H-NMR spectra for pH-dependent hydrolysis of amide bonds at pH 7.4 (red line) and 6.8 (blue line). D) Degradation of the hydrolyzable amide bonds at pH 7.4 and 6.8 (means ± standard deviation (SD), $n = 3$). E) Zeta potentials of viral mimics with different incubation times at pH 7.4, 6.8, and 5.0 (means ± SD, $n = 3$).

at pH 5.0 their lysine-rich corona with highly positive charges to facilitate endosomal escape and nuclear-targeted delivery.

To further simulate viral infection and strengthen programmed targeting at tumor cells, biotinylated amphiphilic dendrons (BADs) as adjuvant components cooperatively assembled with DA-DLPs to generate charge-conversional targeted viral mimics (CTVMs) with receptor-mediated targeting. Polyethylene glycol (PEG, M_w 1500) was introduced into the hydrophilic segments of BADs to improve the water solubility of biotin, and characterizations of BADs were shown in Figures S4 and S18–S24 (Supporting Information). An increasing BADs content (0–30 wt%) in CTVMs just had slight influence on their size and zeta potential, owing to hydration effects of PEG shell in water (**Figure** 4A,B).[49] Given the saturation of biotin receptor on cell membranes and certain obstruction of PEG on cellular uptake,[50–52] we selected an optimal component ratio according to quantitative analysis of the receptor-mediated internalization using fluorescence activated cell sorting (FACS). In this study, hydrophobic doxorubicin (DOX) was used as a model drug encapsulated into the hydrophobic cores of CTVMs, since DOX had inherent

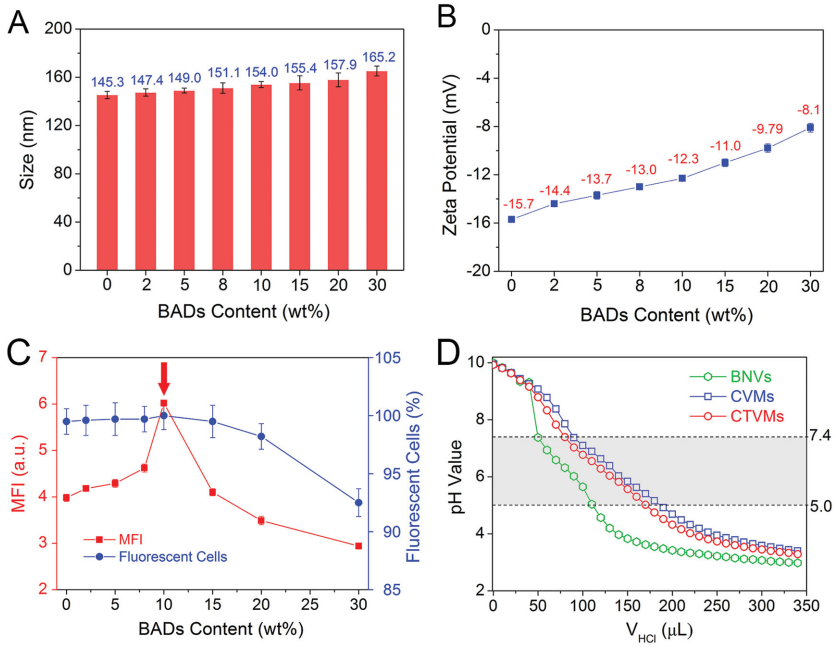

Figure 4. Appropriate proportion for coassembly of DA-DLPs and BADs into the charge-conversional targeted viral mimics. A) Size variations of supramolecular dendritic assemblies containing different BADs contents (0–30 wt%). B) Zeta potential variations of supramolecular dendritic assemblies with different BADs contents from 0 to 30 wt%. C) Quantitative MFI value and percentage of fluorescent cells after exposure to the supramolecular dendritic assemblies containing fluorescent DOX with different BADs contents from 0 to 30 wt%. D) Titration curves of BNVs (self-assembly of BADs), CVMs, and CTVMs (1 mg mL^{-1}, 3 mL) for buffer capacity using 0.01 mol L^{-1} HCl.

fluorescence and good antitumor activity to several tumors; and 4T1 breast tumor cell line was used as a representative cell line of biotin receptor overexpressed tumor cell lines. As shown in FACS results (Figure 4C), with the increase of BADs content, DOX mean fluorescence intensity (MFI) of 4T1 cells first increased to the maximum at 10 wt% BADs, and then gradually decreased due to the saturation of biotin receptor and increased PEG hydration shells. Since the internalization mediated by CTVMs (90 wt% DA-DLPs and 10 wt% BADs) improved over 50% as compared to CVMs, they were selected as a preferred composition mimicking the viral internalization. In addition, incorporated BADs (10 wt%) did not affect the buffer capacity of CTVMs, which had close relationship with endosomal escape by proton-sponge effect at the range from 5.0 to 7.4 (Figure 4D). Collectively, coassembly of DA-DLPs and BADs into CTVMs with virus-like infection and tumor-specific targeting became achievable.

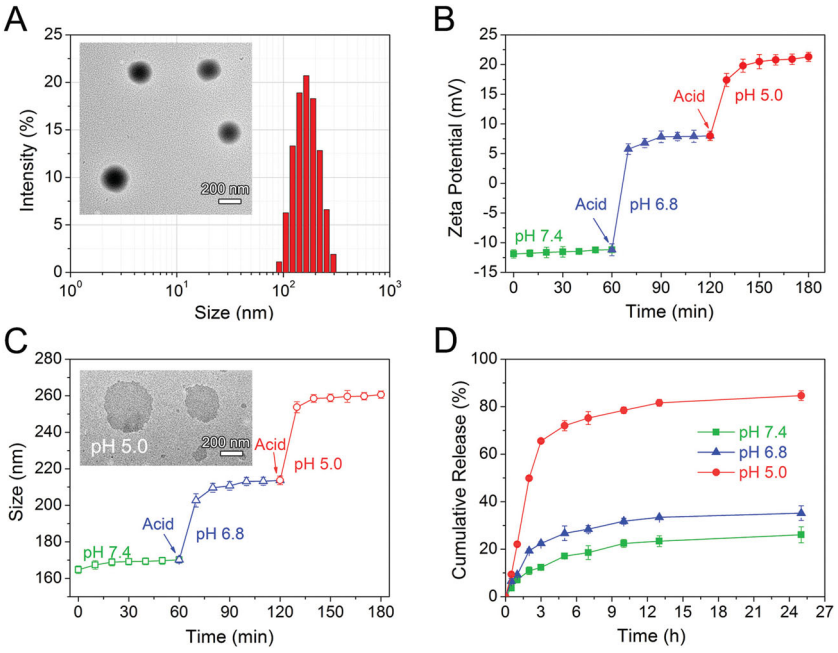

Figure 5. pH-dependent features and in vitro release of D-CTVMs. A) Size distribution and TEM image of D-CTVMs at pH 7.4. B) Zeta potential changes of D-CTVMs at pH 7.4, 6.8, and 5.0. C) Size changes of D-CTVMs at pH 7.4, 6.8, and 5.0. D) DOX release profiles of D-CTVMs at pH 7.4, 6.8, and 5.0 for 25 h with 37 °C, respectively (means ± SD, $n = 3$).

To determine more virus-like properties of CTVMs for encapsulation and controlled release of bioactive molecules, DOX-loaded CTVMs (D-CTVMs) were well prepared and characterized. D-CTVMs exhibited as well-defined nanostructures of ≈170 nm diameter (**Figure 5**A). The DOX loading content was about 10.3%, and loading efficiency was about 44.7%. It was noted that D-CTVMs maintained the charge-tunable features: negative charges (≈–12.0 mV) at pH 7.4, positive charges (≈+8.0 mV) at pH 6.8 and more positive charges (≈+21.5 mV) at pH 5.0 (Figure 5B). Interestingly, the size of D-CTVMs gradually grew larger from 170 to 260 nm with the decrease of pH value, which was attributed to the hydrophilic variations of the amphiphilic dendrons with the dropping of DA and the protonation of amino groups at lower pH conditions; and the incompact nanostructure of D-CTVMs at pH 5.0 would be more advantageous to drug release (Figure 5C).[53] In addition, D-CTVMs were stable in phosphate buffer solution (PBS) at pH 7.4 for 2 d without significant changes on their size and zeta potential (Figure S33, Supporting Information). The in vitro release profiles showed the half-life of DOX release at pH 5.0 to be within 2 h, but the amount of DOX release was only around 20% at pH 7.4 after 25 h (Figure 5D). These results indicated that most of DOX were wrapped into the hydrophobic pocket of CTVMs at pH 7.4 and 6.8, while the lower pH value of pH 5.0 indeed could accelerate the DOX release.[54] Consequently, we had enough reason to believe that D-CTVMs had hierarchically targeted potentials, including passive targeting by EPR effect, tumor extracellular targeting via their charge-tunable shells, receptor-mediated active targeting, endosomal escape and nuclear delivery based on the high positive charges surrounding supramolecular dendritic assemblies.

Once the successful nanofabrication of DOX-loaded viral mimics was confirmed, we immediately turned to evaluate their utility for virus-mimicking delivery in vitro and in vivo. To better clarify the advantages of multifunctional viral mimics for virus-like infection, we constructed a family of drug-loaded ill-defined viral mimics as controls, and the names of these groups (D-PVMs, D-PTVMs, D-CVMs, and D-NTVMs) for in vitro studies are defined in the text. First, CTVMs were obviously nontoxic to 4T1 tumor cells even at a high concentration with the culture media at pH 7.4 and 6.8 (**Figure 6**A,B). Through comparing the cell viabilities of the D-CVMs group (or the D-CTVMs group) at the different pH conditions, it was clear that the culture medium with lower pH 6.8 caused higher cytotoxicity than that of pH 7.4, because at pH 6.8 the deshielding of the charge-tunable shells resulted in the enhanced cellular uptake. By comparison of D-CVMs and D-CTVMs at the same pH condition, their different cytotoxicities to 4T1 tumor cell line showed that the biotinylated nanovehicles of D-CTVMs had better antitumor effects due to receptor-mediated internalization, and the differences were also observed in D-PVMs and DOX-loaded positively charged targeted viral mimics (D-PTVMs, PTVMs coassembled from 90 wt% DLPs and 10 wt% BADs). The IC_{50} values (the concentration causing 50% growth inhibition) for each group were listed in **Table 1**. Notably, D-CTVMs largely improved the antitumor efficiency of DOX with a low IC_{50} value (≈0.88 μg mL^{-1}) with pH 6.8 culture medium, which was reduced more than ten times as compared with hydrophobic DOX (≈9.43 μg mL^{-1}). And the IC_{50} value of D-CTVMs was comparable to the positive control of doxorubicin hydrochloride (DOX.HCl, IC_{50} ≈0.38 μg mL^{-1}) at pH 6.8 mimicking the tumor extracellular microenvironment.

Encouraged by the considerable delivery efficiency of D-CTVMs, we combined fluorescent sorting and multiple

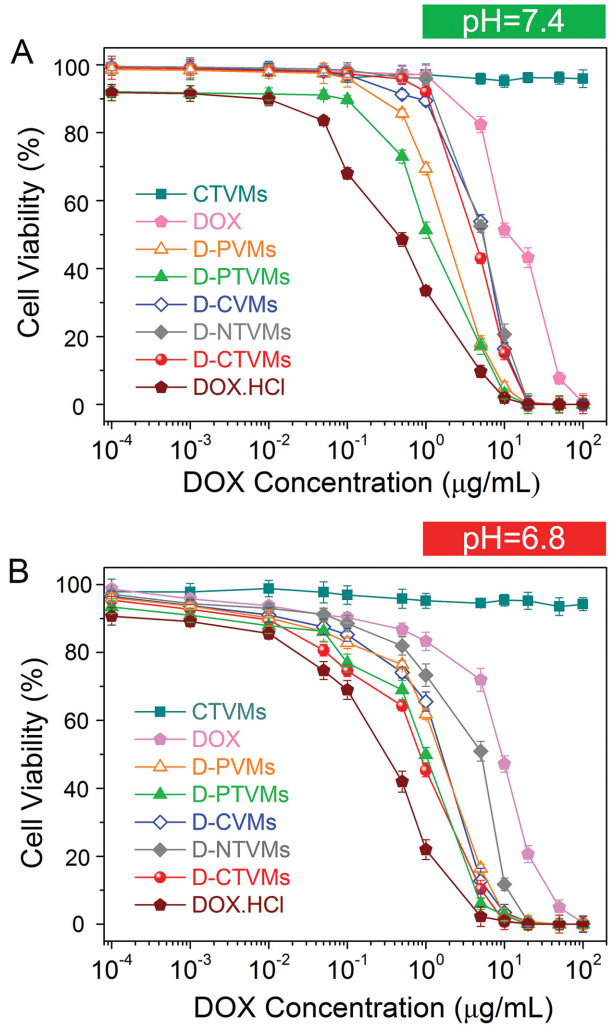

Figure 6. In vitro cytotoxicity of DOX-loaded viral mimics and other control groups to 4T1 cells after incubation for 24 h at A) pH 7.4 and B) pH 6.8 determined by CCK-8 assay (means ± SD, $n = 6$).

fluorescent labeling to disclose their virus-mimicking infections and special merits at cell level. As shown in **Figure 7**A, quantitative MFI of DOX manifested that the DOX internalization by the charge-tunable D-CVMs and D-CTVMs was enhanced more than 100% at pH 6.8 culture medium as compared with them at pH 7.4 ($^*p < 0.01$). Compared with the negatively charged targeted viral mimics (NTVMs, 90 wt% SA-DLPs and 10 wt% BADs), the charge-tunable CTVMs also revealed prominent advantages on the drug internalization. These results indicated the charge-tunable viral mimics could recognize faintly acid tumor microenvironment (pH 6.8–6.0). For another, receptor-mediated infections of biotinylated viral mimics were highlighted by much higher drug internalization mediated by CTVMs than that of CVMs group at pH 6.8; and D-PTVMs internalization was also significantly superior to the D-PVMs group. To further confirm the biotinylated strategy for tumor-specific cellular uptake, 4T1 tumor cells in the (+B)D-CTVMs group were treated with free biotinylated components (10 μg mL^{-1}) for receptor blocking before they were incubated with D-CTVMs.[55] The MFI value of the (+B)D-CTVMs group declined by 36% as compared with the D-CTVMs group at pH 6.8. Thus, it can be seen that receptor-mediated infection played a great role in the enhancement of drug internalization.

Afterward, D-CTVMs were labeled with fluorescein isothiocyanate (FITC) and acidic organelles were stained by Lyso Tracker for monitoring their intracellular fate (Figure 7B). The CLSM images illustrated the FITC-labeled D-CTVMs anchored onto the cell membranes and internalized into 4T1 cells within a short time. After incubation for 3 h at pH 6.8, the FITC-labeled D-CTVMs were entrapped into the acidic organelles such as endosomes and lysosomes (overlap of green fluorescence, red fluorescence, and blue fluorescence). Excitingly, a large amount of DOX escaped from endosomes and dispersed in the cytoplasm at 6 h (disassociation of red fluorescence, green fluorescence, and blue fluorescence), which resulted from their lysine-rich supramolecular structures with high zeta potential and buffer capacity at the lower pH condition in lysosomes. Nuclear delivery is an important consideration for efficient nanocarriers, because many clinical antitumor drugs played their therapeutic roles in the nuclei such as DOX and cisplatin.[42] We further confirmed targeted nuclear delivery of CTVMs by Hoechst 33342 staining (Figure 7C). The CLSM images directly displayed that the nanovehicles containing the charge-tunable components (DA-DLPs) transported more the fluorescent DOX into 4T1 cells with the lower pH culture medium (6.8). Moreover, CTVMs efficiently delivered DOX into the nuclei to exert antitumor activity with 3 h (overlap of red fluorescence and blue fluorescence). The similar phenomena occurred in other groups which usually involved a major part of the charge-tunable DA-DLPs. In line with our previous studies, the lysine-rich supramolecular dendritic system could escape from endosomes and deliver drug into nuclei mimicking viral intracellular delivery.[21,28,40]

The ultimate goal of developing viral mimics is that enhanced in vivo antitumor efficacy and reduced side effects can be achieved by virus-inspired systemic delivery. The in vivo therapeutic efficacy of the D-CTVMs was evaluated in BALB/c mice bearing 4T1 tumor using systemic administration (intravenous injection). The tumor suppression was evaluated by monitoring tumor volume changes (**Figure 8**A). The CTVMs had no obvious effect on tumor growth of BALB/c mice as

Table 1. Drug concentrations at 50% inhibition (IC50) to 4T1 tumor cell line.

Groups	DOX	D-PVMs	D-PTVMs	D-CVMs	D-NTVMs	D-CTVMs	DOX·HCl
IC_{50} (pH 7.4)[a)]	11.60	2.51	1.15	5.51	5.39	4.43	0.47
IC_{50} (pH 6.8)[a)]	9.43	2.04	0.99	2.17	5.11	0.88	0.38

[a)]Determined by CCK-8 assays after incubation with drug or drug-loaded viral mimics for 24 h with different pH conditions (concentration unit: μg mL^{-1}).

ADVANCED FUNCTIONAL MATERIALS
www.afm-journal.de

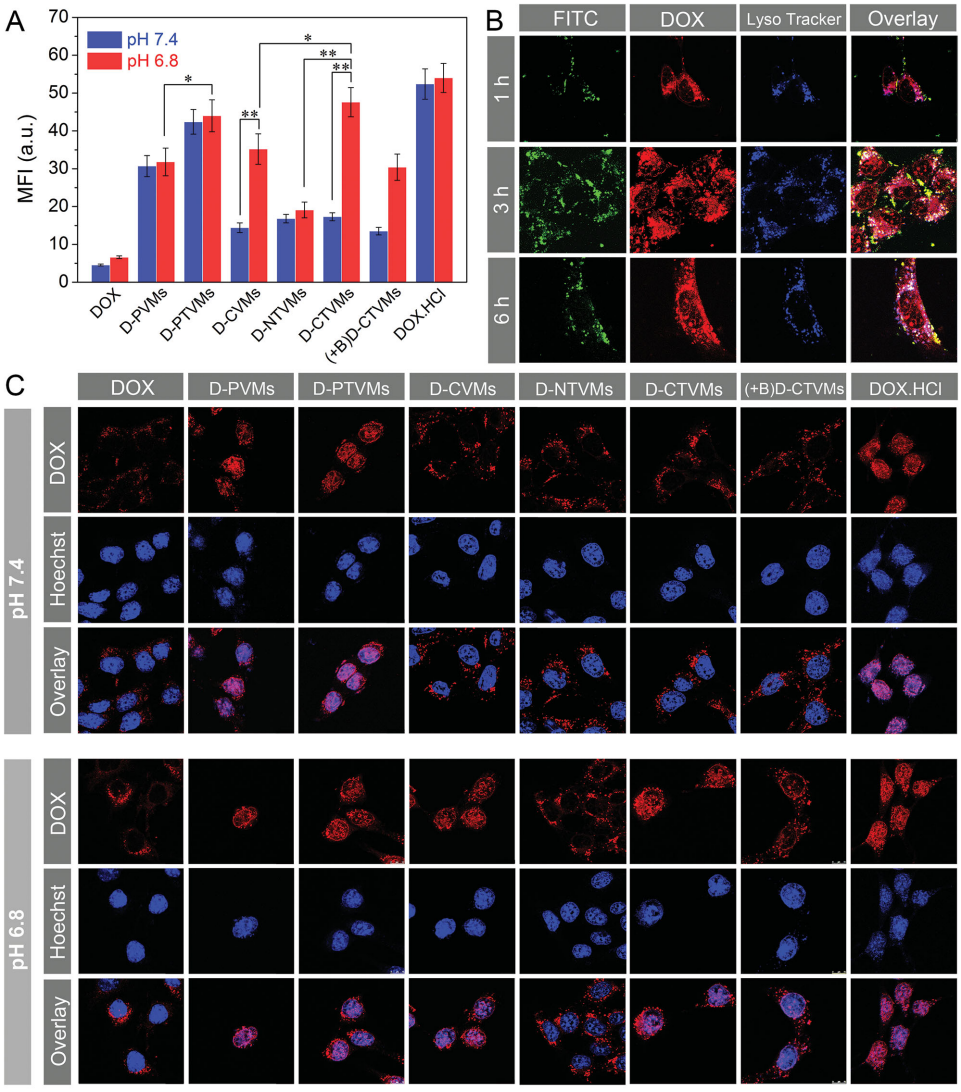

Figure 7. Cellular uptake and intracellular drug delivery to 4T1 tumor cell line. A) MFI (DOX) for quantitative cellular uptake after incubation with DOX-loaded nanovehicles (10 μg mL^{-1} DOX) at different pH conditions for 3 h detected by FACS (means ± SD, $n = 3$, *$p < 0.01$, **$p < 0.001$). B) CLSM images for intracellular tracking of D-CTVMs (5 μg mL^{-1} DOX) at different time points including FITC-labeled CTVMs channel (green), DOX channel (red), Lyso Tracker-stained lysosome channel (blue), and overlay of previous images. C) CLSM images for nuclear delivery of DOX-loaded viral mimics (10 μg mL^{-1} DOX) after incubation with different pH conditions for 3 h.

compared to the saline-administered BALB/c mice. The tumor growth rate in the saline-administered group dramatically increased to 9.6-fold than that in the D-CTVMs-administered group after treatment over 18 d (*$p < 0.001$). Encouragingly, in vivo tumor suppression of D-CTVMs even exceeded the positive control group (administered by water-soluble DOX.HCl) more than three times. Inspection of the tumor growth rates in the D-CVMs group and the D-NTVMs group also indicated the charge-tunable or biotinylated nanovehicles remarkably improved antitumor efficiency of DOX. As shown in Figure 8B, the virus-inspired targeted strategy of D-CTVMs for systemic delivery, which combined viral component and structure simulations, tumor microenvironment targeting, receptor-mediated targeting, and subcellular targeting, did achieve maximum in vivo antitumor effects.

Then, the in vivo therapeutic efficacy and mechanism were also analyzed by histological and immunohistochemical studies (Figure 8C). Haematoxylin and eosin (H&E) staining of tumor slices showed that administration of the D-CTVMs resulted in the most remarkable damage in tumor tissue after treatment, quite differing from superabundant and compact tumor cells in the saline-administered group. Meanwhile, the administration of D-CTVMs very effectively inhibited CD31-positive vessels formation and reduced proliferating Ki67-positive tumor cells as compared with the control groups. More importantly, the D-CTVMs induced the most apoptotic cells (TUNEL-positive cells) in tumor tissue, which was about twofold higher than that of the DOX.HCl group (Figure S39, Supporting Information).

Next, we started to investigate in vivo fate of D-CTVMs after systemic administration to disclose the merits of viral mimics.

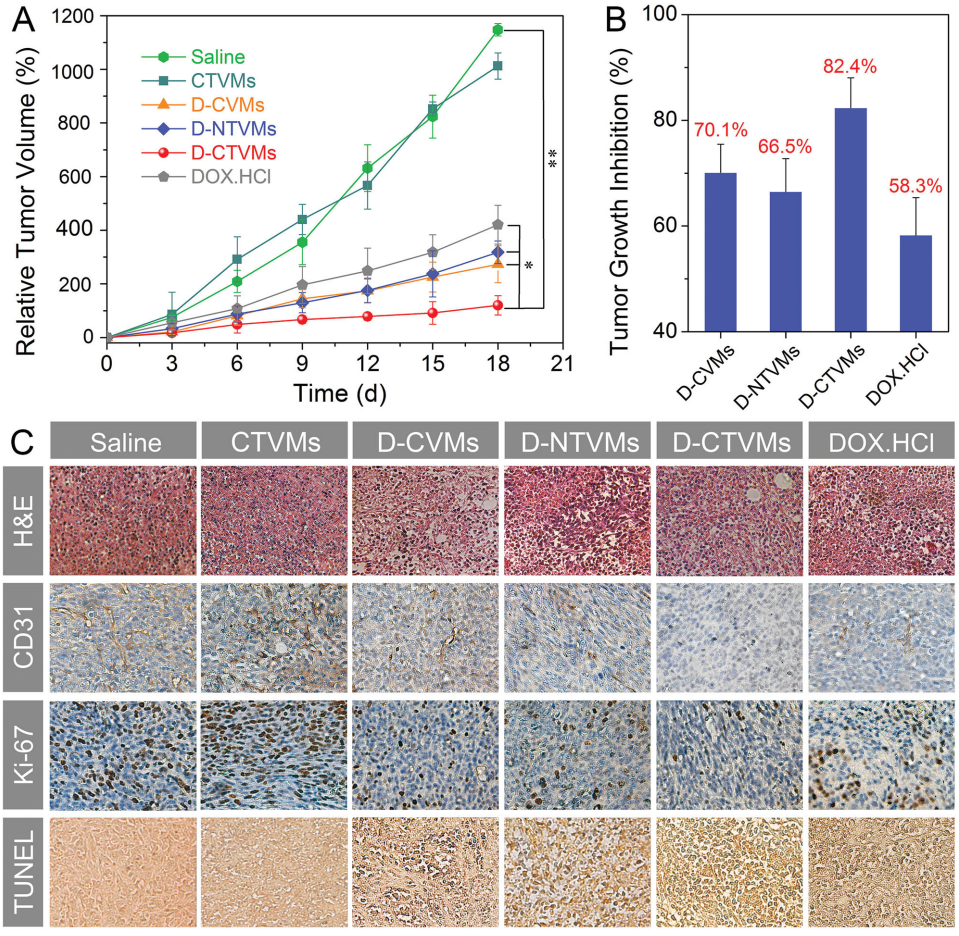

Figure 8. In vivo therapeutic efficacy against BALB/c mice bearing 4T1 tumor. A) Tumor volume changes of BALB/c mice bearing 4T1 tumor administered with saline (control), CTVMs, D-CVMs, D-NTVMs, D-CTVMs, and DOX.HCl by intravenous injection (5 mg DOX kg^{-1}, means ± SD, $n = 6$, $^{**}p < 0.001$, $^{*}p < 0.01$). B) Tumor growth inhibition after treatment with different administrations over 18 d. C) Histological and immunohistochemical images of H&E, CD31, Ki-67, and TUNEL assays for tumor tissues. CD31-positive vessels and Ki-67-positive cells are stained brown, and TUNEL-positive cells are stained blue.

To evaluate the resistance to protein adsorption of CTVMs, we determined how much proteins absorbed onto the viral mimics after exposure to bovine serum albumin (BSA) solution at pH 7.4 and 6.8, respectively. The results showed that both at the pH 7.4 and 6.8, little proteins absorbed onto the negatively charged NTVMs, while the significant protein adsorption was detected in the positively charged PTVMs group (**Figure 9**A). As speculated, CTVMs resisted the protein adsorption at normal physiological pH condition due to their surrounding negative charges, and low pH condition (6.8) could trigger the charge conversion of CTVMs to activate protein interactions immediately. The plasma drug concentration versus time profiles after intravenous injection of DOX.HCl solution and various DOX-loaded nanovehicles (D-CVMs, D-NTVMs, and D-CTVMs) at a single dose of 10 mg kg^{-1} to BALB/c mice are shown in Figure 9B, and pharmacokinetic parameters are listed in Table S1 (Supporting Information).[56] Compared with the DOX.HCl solution having area under the curve (AUC, 40.58) and half-life ($t_{1/2}$, 0.38 h), the VMs-encapsulated DOX showed many advantages as follows: D-CVMs, D-NTVMs, and D-CTVMs (i) increased AUC of 129.55 (3.19-fold), 197.08 (4.86-fold), and 245.50 (6.05-fold), (ii) and enlarged $t_{1/2}$ of 2.31 (6.08-fold), 5.82 (15.32-fold), and 6.65 (17.50-fold), respectively. These results indicated that viral mimics indeed significantly prolonged the blood circulation time of drug because of their stealthy surfaces.

Subsequently, fluorescent imaging for drug distribution was carried out to confirm the in vivo tumor targeting of D-CTVMs (Figure 9C). Comprehensive analysis of each group at all monitoring time points indicated that these viral mimics were more favorable for the DOX accumulation in solid tumors by EPR effect than free DOX·HCl. Comparing the DOX fluorescence located at the tumor site, the strongest intensity and largest area were observed in the D-CTVMs group owing to the promoted tumor accumulation by synergetic targeting. The ex vivo semiquantitative DOX content in different organs and tumors also indicated that D-CTVMs were a predominant delivery system for solid tumor targeting, but less accumulation of water-soluble DOX·HCl may be related to its drug metabolism (Figure 9D).

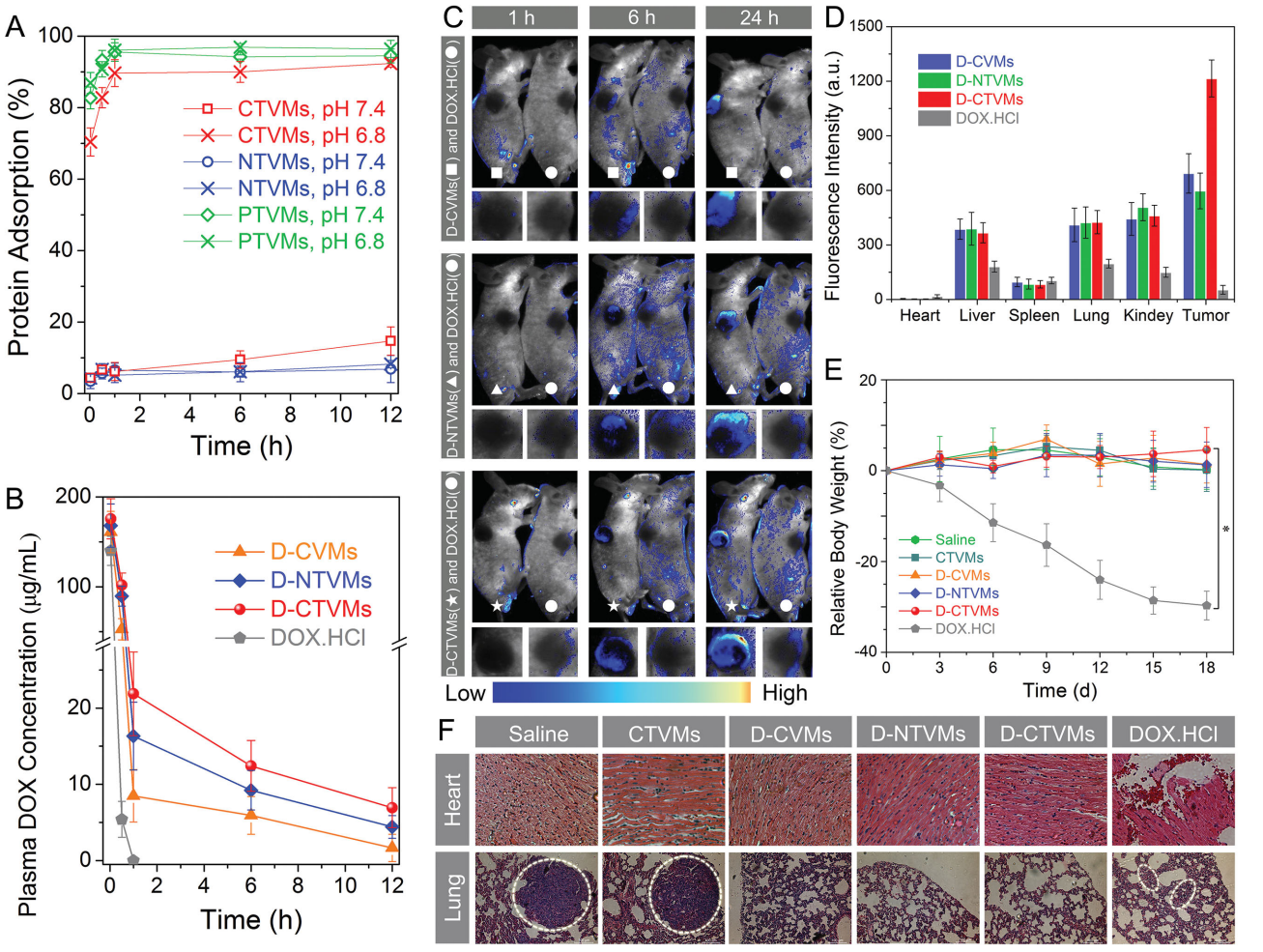

Figure 9. In vivo tumor targeted delivery and reduced side effects. A) Protein adsorption on the viral mimics after incubation with different time points and pH conditions at 37 °C (means ± SD, $n = 3$). B) Pharmacokinetic profiles after intravenous injection of DOX.HCl and various DOX-loaded nanovehicles in BALB/c mice at a drug dose of 10 mg kg^{-1} (means ± SD, $n = 3$). C) Fluorescent images of nude mice bearing 4T1 tumor after different administrations of DOX.HCl, D-CVMs, D-NTVMs, and D-CTVMs using intravenous injection at different monitoring times. D) Ex vivo DOX fluorescence intensity of organs and tumors after intravenous injection for 24 h. E) Body weight changes of BALB/c mice bearing 4T1 tumor with different administrations over 18 d ($n = 6$, *$p < 0.001$). F) Images of H&E assays for hearts and lungs after treatment with different administrations over 18 d.

As the BALB/c mice finished the course of treatment, BALB/c mice treated by DOX.HCl showed a significant reduction in body weight by 30% due to drug side effects (Figure 9E). However, no significant difference in body weight of BALB/c mice was observed after administrations with the viral mimics–based delivery systems, as well as the saline-administered group. Furthermore, the histological analysis provided another evidences for minimizing the DOX toxicity to the heart tissue with the VMs-packaged DOX (Figure 9F). It was well known that pulmonary metastasis was the most typical and fatal tumor metastasis, and the marked pulmonary metastasis of saline-administered group was shown in the H&E stained lung slice, which was marked by white line.[56,57] In contrast, few metastasis sites were observed in the lung of the D-CTVMs group, even better than the DOX.HCl group. It was concluded that the charge-tunable targeted viral mimics successfully broke through the biological barriers in drug delivery and offered the satisfactory therapeutic effects as well as reduced side effects.

3. Conclusions

In summary, we demonstrated a virus-inspired strategy to build lipopeptide-based mimics of viral architectures and infections for overcoming key biological barriers and navigating systemic delivery. These virus-inspired mimics have virus-like components, well-defined nanostructures, and negatively charged surface at normal pH condition, which are able to resist protein adsorption, prolong blood circulation time, and transport the drug to tumor site by passive targeting (EPR effect). More importantly, synergetic effects of tumor extracellular targeting (charge-tunable shielding) and receptor-mediated active targeting (biotin moieties) largely enhanced the drug accumulation at tumor site and tumor cell internalization. After adequate exposure of amino groups in CTVMs, the lysine-rich supramolecular dendritic systems smoothly achieved endosomal escape and nuclear delivery to exert the antitumor activity of DOX. In vitro and in vivo results confirmed the multifunctional viral

mimics provided much better tumor treatment effects as compared with positive control group (DOX.HCl) and other control groups, including the aspects of tumor growth inhibition, side effects, and tumor metastasis. As a result, the versatile viral mimics successfully take advantages of viral structural/functional simulations and tumorous unique features for achieving highly efficient systemic delivery. We hope that this work will set the stage for the development of novel viral mimics and efficient tumor therapy.

Supporting Information

Supporting Information is available from the Wiley Online Library or from the author.

Acknowledgements

Z.Z. and X.Z. contributed equally to this work. This work was supported by National Natural Science Foundation of China (NSFC, 51133004 and 81361140343), National Basic Research Program of China (973 program, 2011CB606206), Joint Sino-German Research Project (GZ756 and GZ905), the Department of Science and Technology from Sichuan Province (2013FZ0003), and Scientific Research Foundation for Youth Scholars from Sichuan University (2015SCU11037). The authors thank Prof. Xuehua Jiang for the kind help on pharmacokinetics. The authors also thank Jiao Lu and Na Li for the helps on biological experiments.

Received: May 18, 2015
Revised: June 24, 2015
Published online: July 16, 2015

[1] C. Sanchez, H. Arribart, M. M. G. Guille, *Nat. Mater.* **2005**, *4*, 277.
[2] K. S. Liu, L. Jiang, *ACS Nano* **2011**, *5*, 6786.
[3] A. R. Studart, *Angew. Chem. Int. Ed.* **2015**, *54*, 3400.
[4] U. G. K. Wegst, H. Bai, E. Saiz, A. P. Tomsia, R. O. Ritchie, *Nat. Mater.* **2015**, *14*, 23.
[5] M. A. Kay, J. C. Glorioso, L. Naldini, *Nat. Med.* **2001**, *7*, 33.
[6] Y. J. Ma, R. J. M. Nolte, J. J. L. M. Cornelissen, *Adv. Drug Delivery Rev.* **2012**, *64*, 811.
[7] G. Zuber, E. Dauty, M. Nothisen, P. Belguise, J. P. Behr, *Adv. Drug Delivery Rev.* **2001**, *52*, 245.
[8] E. Mastrobattista, M. A. E. M. van der Aa, W. E. Hennink, D. J. A. Crommelin, *Nat. Rev. Drug Discovery* **2006**, *5*, 115.
[9] J. W. Yoo, D. J. Irvine, D. E. Discher, S. Mitragotri, *Nat. Rev. Drug Discovery* **2011**, *10*, 521.
[10] K. Miyata, N. Nishiyama, K. Kataoka, *Chem. Soc. Rev.* **2012**, *41*, 2562.
[11] E. Wagner, *Acc. Chem. Res.* **2012**, *45*, 1005.
[12] Y. Zhao, F. Sakai, L. Su, Y. J. Liu, K. C. Wei, G. S. Chen, M. Jiang, *Adv. Mater.* **2013**, *25*, 5215.
[13] C. Schatz, S. Louguet, J. F. Le Meins, S. Lecommandoux, *Angew. Chem., Int. Ed.* **2009**, *48*, 2572.
[14] Y. Ruff, T. Moyer, C. J. Newcomb, B. Demeler, S. I. Stupp, *J. Am. Chem. Soc.* **2013**, *135*, 6211.
[15] R. Ni, Y. Chau, *J. Am. Chem. Soc.* **2014**, *136*, 17902.
[16] Y. Aoyama, T. Kanamori, T. Nakai, T. Sasaki, S. Horiuchi, S. Sando, T. Niidome, *J. Am. Chem. Soc.* **2003**, *125*, 3455.
[17] Y. B. Lim, E. Lee, Y. R. Yoon, M. S. Lee, M. Lee, *Angew. Chem. Int. Ed.* **2008**, *47*, 4525.
[18] Y. T. Niu, M. H. Yu, S. B. Hartono, J. Yang, H. Y. Xu, H. W. Zhang, J. Zhang, J. Zou, A. Dexter, W. Y. Gu, C. Z. Yu, *Adv. Mater.* **2013**, *25*, 6233.
[19] S. D. Perrault, W. M. Shih, *ACS Nano* **2014**, *8*, 5132.
[20] F. Boato, R. M. Thomas, A. Ghasparian, A. Freund-Renard, K. Moehle, J. A. Robinson, *Angew. Chem. Int. Ed.* **2007**, *46*, 9015.
[21] X. H. Xu, H. Yuan, J. Chang, B. He, Z. W. Gu, *Angew. Chem. Int. Ed.* **2012**, *51*, 3130.
[22] J. Chang, X. H. Xu, H. P. Li, Y. T. Jian, G. Wang, B. He, Z. W. Gu, *Adv. Funct. Mater.* **2013**, *23*, 2691.
[23] G. F. Walker, C. Fella, J. Pelisek, J. Fahrmeir, S. Boeckle, M. Ogris, E. Wagner, *Mol. Ther.* **2005**, *11*, 418.
[24] E. S. Lee, D. Kim, Y. S. Youn, K. T. Oh, Y. H. Bae, *Angew. Chem. Int. Ed.* **2008**, *47*, 2418.
[25] P. S. Xu, S. Y. Li, Q. Li, E. A. Van Kirk, J. Ren, W. J. Murdoch, Z. J. Zhang, M. Radosz, Y. Q. Shen, *Angew. Chem. Int. Ed.* **2008**, *47*, 1260.
[26] R. Roy, D. J. Jerry, S. Thayumanavan, *Biomacromolecules* **2009**, *10*, 2189.
[27] N. P. Truong, W. Y. Gu, I. Prasadam, Z. F. Jia, R. Crawford, Y. Xiao, M. J. Monteiro, *Nat. Commun.* **2013**, *4*, 1902.
[28] X. H. Xu, Y. K. Li, H. P. Li, R. Liu, M. M. Sheng, B. He, Z. W. Gu, *Small* **2014**, *10*, 1133.
[29] Y. Y. He, Y. Nie, G. Cheng, L. Xie, Y. Q. Shen, Z. W. Gu, *Adv. Mater.* **2014**, *26*, 1534.
[30] R. Waehler, S. J. Russell, D. T. Curiel, *Nat. Rev. Genet.* **2007**, *8*, 573.
[31] V. Percec, D. A. Wilson, P. Leowanawat, C. J. Wilson, A. D. Hughes, M. S. Kaucher, D. A. Hammer, D. H. Levine, A. J. Kim, F. S. Bates, K. P. Davis, T. P. Lodge, M. L. Klein, R. H. DeVane, E. Aqad, B. M. Rosen, A. O. Argintaru, M. J. Sienkowska, K. Rissanen, S. Nummelin, J. Ropponen, *Science* **2010**, *328*, 1009.
[32] S. Sevenson, D. A. Tomalia, *Adv. Drug Delivery Rev.* **2012**, *64*, 102.
[33] S. D. Zhang, R. O. Moussodia, H. J. Sun, P. Leowanawat, A. Muncan, C. D. Nusbaum, K. M. Chelling, P. A. Heiney, M. L. Klein, S. Andre, R. Roy, H. J. Gabius, V. Percec, *Angew. Chem. Int. Ed.* **2014**, *53*, 10899.
[34] F. M. Veronese, G. Pasut, *Drug Discovery Today* **2005**, *10*, 1451.
[35] Y. Y. Yuan, C. Q. Mao, X. J. Du, J. Z. Du, F. Wang, J. Wang, *Adv. Mater.* **2012**, *24*, 5476.
[36] Z. X. Zhou, Y. Q. Shen, J. B. Tang, M. H. Fan, E. A. Van Kirk, W. J. Murdoch, M. Radosz, *Adv. Funct. Mater.* **2009**, *19*, 3580.
[37] E. Gullotti, Y. Yeo, *Mol. Pharm.* **2009**, *6*, 1041.
[38] Y. H. Li, J. Wang, M. G. Wientjes, J. L. S. Au, *Adv. Drug Delivery Rev.* **2012**, *64*, 29.
[39] J. D. Byrne, T. Betancourt, L. Brannon-Peppas, *Adv. Drug Delivery Rev.* **2008**, *60*, 1615.
[40] X. H. Xu, Y. T. Jian, Y. K. Li, X. Zhang, Z. X. Tu, Z. W. Gu, *ACS Nano* **2014**, *8*, 9255.
[41] L. Rajendran, H. J. Knolker, K. Simons, *Nat. Rev. Drug Discovery* **2010**, *9*, 29.
[42] M. H. Sui, W. W. Liu, Y. Q. Shen, *J. Controlled Release* **2011**, *155*, 227.
[43] X. Zhang, Z. J. Zhang, X. H. Xu, Y. K. Li, Y. C. Li, Y. T. Jian, Z. W. Gu, *Angew. Chem. Int. Ed.* **2015**, *54*, 4289.
[44] K. K. Ng, J. F. Lovell, G. Zheng, *Acc. Chem. Res.* **2011**, *44*, 1105.
[45] Y. Lee, S. Fukushima, Y. Bae, S. Hiki, T. Ishii, K. Kataoka, *J. Am. Chem. Soc.* **2007**, *129*, 5362.
[46] P. S. Xu, E. A. Van Kirk, Y. H. Zhan, W. J. Murdoch, M. Radosz, Y. Q. Shen, *Angew. Chem. Int. Ed.* **2007**, *46*, 4999.
[47] J. Z. Du, X. J. Du, C. Q. Mao, J. Wang, *J. Am. Chem. Soc.* **2011**, *133*, 17560.
[48] M. B. van Eldijk, J. C. Y. Wang, I. J. Minten, C. L. Li, A. Zlotnick, R. J. M. Nolte, J. J. L. M. Cornelissen, J. C. M. van Hest, *J. Am. Chem. Soc.* **2012**, *134*, 18506.

[49] O. Garbuzenko, Y. Barenholz, A. Priev, *Chem. Phys. Lipids* **2005**, *135*, 117.
[50] H. Hatakeyama, H. Akita, H. Harashima, *Adv. Drug Delivery Rev.* **2011**, *63*, 152.
[51] D. W. Pack, A. S. Hoffman, S. Pun, P. S. Stayton, *Nat. Rev. Drug Discovery* **2005**, *4*, 581.
[52] K. Qi, Q. G. Ma, E. E. Remsen, C. G. Clark, K. L. Wooley, *J. Am. Chem. Soc.* **2004**, *126*, 6599.
[53] S. S. Naik, J. G. Ray, D. A. Savin, *Langmuir* **2011**, *27*, 7231.
[54] T. Kim, T. Rothmund, T. Kissel, S. W. Kim, *J. Controlled Release* **2011**, *152*, 110.
[55] H. Yuan, K. Luo, Y. S. Lai, Y. J. Pu, B. He, G. Wang, Y. Wu, Z. W. Gu, *Mol. Pharm.* **2010**, *7*, 953.
[56] L. Ma, F. Reinhardt, E. Pan, J. Soutschek, B. Bhat, E. G. Marcusson, J. Teruya-Feldstein, G. W. Bell, R. A. Weinberg, *Nat. Biotechnol.* **2010**, *28*, 341.
[57] M. Y. Wu, Q. S. Meng, Y. Chen, P. F. Xu, S. J. Zhang, Y. P. Li, L. X. Zhang, M. Wang, H. L. Yao, J. L. Shi, *Adv. Funct. Mater.* **2014**, *24*, 4273.